JCTC Journal of Chemical Theory and Computation

Lattice-Boltzmann Simulations of Ionic Current Modulation by DNA Translocation

Sylvain Reboux,[†] Fabrizio Capuani,[‡] Nélido González-Segredo, and Daan Frenkel*

FOM Institute for Atomic and Molecular Physics, Kruislaan 407, 1098 SJ Amsterdam, The Netherlands

Received December 31, 2005

Abstract: We present a numerical study of the effect of DNA translocation on the ionic current through a nanopore. We use a coarse-grained model to solve the electrokinetic equations at the Poisson−Boltzmann level for the microions, coupled to a lattice-Boltzmann equation for the solvent hydrodynamics. In most cases, translocation leads to a reduction in the ionic current. However, at low salt concentrations (large screening lengths) we find ionic current enhancement due to translocation. In an unstructured pore, translocation of the helical charge distribution of the DNA has no effect on the ionic current. However, if a localized charge probe is placed on the wall of the nanopore, we observe ionic current modulations that, though weak, should be experimentally observable.

1. Introduction

The subtle and often counterintuitive effects underlying many electrokinetic phenomena, and their relevance in the behavior of many synthetic and biological complex fluids, make their study one of both practical and fundamental interest.[1,2] Electrokinetic effects such as electro-osmosis and electrophoresis can be used to control the transport of small molecules and colloids;[3] as microfluidic devices become ever more prevalent, there is an increasing number of electrokinetic effects that can be exploited for selective molecular transport.[4] An important example is the translocation of highly charged biopolymers such as DNA and RNA through biological or synthetic nanoscale pores. This topic has excited much experimental and theoretical interest[5−9] not only because of its potential implications for DNA sequencing but also because of the importance of biopolymer translocation in living organisms. Biopolymer translocation is involved, for example, in the transport of transcribed RNA out of the cell nucleus and viral injection of DNA into a host cell. The idea behind DNA sequencing using translocation through nanopores is to use biological or synthetic pores such as nanosensors to characterize very locally the spatial extent and charge distribution of the translocating polymer. This is done by measuring electric current fluctuations under a constant voltage bias.[8]

Experiments[9] and atomistic simulations[10−12] have been used to gain insight in the factors that determine the relation between the local structure of the translocating biopolymer and the associated ionic current. However, the interpretation of the experimental data in terms of a microscopic model is often not unique. Fully atomistic simulations make it possible to relate macroscopic observables, such as current modulations, to microscopic properties of the system under study, but such simulations are computationally very expensive. This makes them less suited for a systematic study of the effect of the different parameters (such as pore size and ionic strength) that affect the translocation current. In virtually all cases of practical interest, electrokinetic phenomena occur in confined systems of a rather complex geometry; as a consequence, the analytical solution of continuum—in particular, electrokinetic—equations can usually not be obtained. In addition, the dynamics of translocation is determined by a number of distinct characteristic lengths and times that may differ by several orders of magnitude: ionic radius, Debye screening length, channel/pore size and polyelectrolyte size, time of formation of the electrical double layer (EDL), and the transient time for the onset of convective currents. The

* Corresponding author e-mail: frenkel@amolf.nl.
[†] Current address: Division of Applied Mathematics, University of Nottingham, Nottingham NG7 2RD, U.K.
[‡] Current address: FIRC Institute for Molecular Oncology, Via Adamello 16, 20139 Milan, Italy.

10.1021/ct050340g CCC: $33.50 © 2006 American Chemical Society
Published on Web 03/22/2006

need to span these scales may render atomistic simulation unpractical.

Mesoscopic ('coarse-grained') models for fluid dynamics can offer an alternative to atomistic simulation in the study of electrokinetic phenomena. To be more precise, coarse-grained models are useful to study phenomena on length and time scales where the details of a fully atomistic description can be represented by a small number of parameters. There exist several coarse-grained, mesoscopic methods to model hydrodynamics. Most notable among these are Dissipative Particle Dynamics (DPD), Stochastic Rotation Dynamics (SRD), and Lattice-Boltzmann (LB) methods. Dissipative Particle Dynamics can be viewed as a coarse-grained version of Molecular Dynamics, whereby mesoscopic particles representing elements of solvent move under the influence of conservative, friction, and stochastic forces.[13−15] Stochastic Rotation Dynamics[16,17] models the solvent as a viscous gas that undergoes stochastic many-body collisions. The interactions among solutes and between solute and solvent are described by conservative forces. Finally, the Lattice-Boltzmann (LB) method employs a coarse-grained lattice-gas cellular automaton model for a fluid which approximately solves the (continuum) Boltzmann transport equation, which in turn describes hydrodynamics (for details, see e.g. refs 18−20).

The relative merits of the different coarse-grained approaches to mesoscopic fluid dynamics depend not only on the nature of the problem but also on the state of development of the various techniques. At present, there are versions of the Lattice-Boltzmann method that can be used to model electrokinetic effects. For the study reported in the present manuscript, we employ the approach described in ref 21. The LB scheme of ref 21 integrates a Boltzmann transport equation for the solvent to a local diffusion equation for the charge dynamics. In ref 21 it is shown that this approach provides an excellent description of the sedimentation of charged colloids.

There also exists a version of DPD that takes charge transport into account.[15] However, unlike the LB method, DPD introduces an additional length scale into the description of electrolyte solutions, namely the size of the charged mesoparticles. These mesoions are larger than simple ions yet must be much smaller than the Debye screening length in order for charge modulations not to become obscured by spurious structural correlations. This makes it nontrivial to achieve a proper separation of length scales in DPD simulations of electrolytes. The LB method also has advantages when compared with more macroscopic approaches, such as a direct solution of the Navier−Stokes equation: the LB scheme tends to be numerically more stable, and it is straightforward to impose complicated boundary conditions. To our knowledge, there exists no viable version of SRD for electrolyte solutions.

The LB method that we use in the present paper treats electrostatics at the level of the nonlinear Poisson−Boltzmann equation, thus allowing us to model electrokinetic effects at high surface-charge densities. It should be noted that the Poisson−Boltzmann description does not account for correlation effects associated with the finite sizes of the salt ions nor for explicit charge correlations. Hence, physical phenomena that are sensitive to the discrete nature of the individual ions, such as like-charge attraction[33] or ion adsorption to highly charged polyelectrolytes (see e.g. ref 34), will not be captured by this formalism. However, our aim is to model electrokinetics at the simplest possible level in order to explore to what extent a purely continuum description can be used to describe the rather complex electrokinetic effects associated with DNA translocation. In this respect, our calculations can be considered as a "baseline" for more detailed (atomistic) simulations.

Explicit description of the individual ions is of course possible in more atomistic simulations (see e.g. ref 22), but the latter approach is computationally more expensive. Of course, the description of the fluid motion by hydrodynamics is also an approximation. However, one of the surprises in the study of the dynamics of simple liquids is that continuum hydrodynamics provides a good description of motions in fluids, even at the nanoscale. This is illustrated, for example, by the success of the Stokes−Einstein relation that connects the diffusion coefficient of microscopic particles to the hydrodynamic friction coefficient. This relation works extremely well for small colloids and even (to within a factor two) for atoms.

The remainder of this paper is organized as follows. In section II we present our model for a translocating DNA oligomer, and we discuss the equations that govern charge and mass transport. In section III we validate the numerical solution of the electrokinetic equations for the given boundary conditions (translocating rod) by (a) comparing the computed equilibrium profiles for the electrical double layer with the corresponding analytical solutions, in the low-charge regime, and (b) by showing that, in the low-salt and high-charge regime, the model correctly reproduces Manning condensation. In section IV, we show that DNA translocation may lead to both reduction and enhancement of the ionic current. Current enhancement is a low-salt and high-charge effect. We give a simple analytical estimate for this effect that matches well with our numerical calculations. In section V we address the possibility of detecting a signature of the DNA charge distribution in the ionic current. We show that current modulation during translocation should be observable, provided that there is a localized charge placed just inside the wall of the pore. In that case, we find that upon moving both single-stranded and double-stranded DNA through a nanopore, the ionic current undergoes modulations as a result of the overlapping of the electrical double layer of the DNA with that of the "probe" charge.

II. The Model

The length of nanopores, be they synthetic or biological, is usually less than the persistence length of most biopolymers. Hence, for a local description of the pore plus translocating biopolymer, it is reasonable to approximate the biomolecule by a rigid rod. This approximation is certainly justified for double-stranded DNA, a semiflexible polymer with a persistence length of ca. 50−100 nm. In what follows, we simplify the description even further by modeling the DNA-pore system as a nondeformable cylinder that is concentric

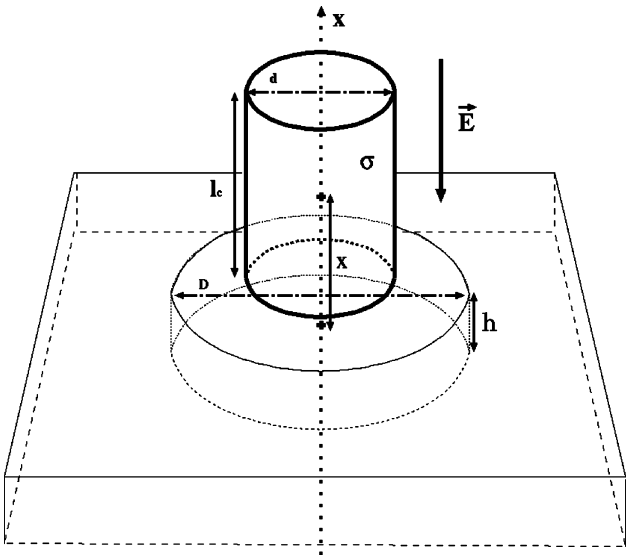

Figure 1. Sketch of the geometry of a rodlike polyelectrolyte of length *L* and diameter *d* translocating through a hole of height *h* and diameter *D*. The surface charge density of the polyelectrolyte is denoted by σ. The applied electric field **E** is parallel to the axis of the rodlike polymer.

with a cylindrical pore in an electrically neutral, rigid slab (see Figure 1). We studied two charge distributions on the surface of the cylinder: (a) homogeneous and (b) helical line charge on a single and a double helix.

In some of the experiments that probe the modulation of ionic current by DNA translocation, one end of a DNA oligomer is attached to a microbead that is trapped by an optical tweezer; the DNA chain is then straightened by the applied electric field. The position of the DNA in the pore can be varied at will. When the DNA is kept fixed, an applied electric field will first induce a transient current that then settles down to a steady-state value. In our simulations, we reproduce this scenario by positioning the charged cylinder at a fixed position close to or in the pore. We then let the surrounding electrolyte relax to steady state under the applied electric field.

The electrolyte solution in which the cylinder is immersed contains two oppositely charged microion species of concentration ρ^k, $k = +, -$, and negligible molecular size. The ions diffuse in a solvent of number density ρ. We assume that the flow of the solvent obeys the Navier−Stokes equation for incompressible fluids. The electrolyte can undergo two types of dynamics: (a) short-range, diffusive mass transport and (b) long-range, driven transport. To maintain charge neutrality of the total system (DNA + electrolyte solution), the electrolyte must contain an excess charge of counterions that matches the total charge on the cylinder.

Before applying an external uniform electric field **E** parallel to the longitudinal axis of the DNA, we allow a period of time for the formation of the electrical double layer, at which the electrolyte reaches electrostatic equilibrium. Once the external field is switched on, it exerts a force on those fluid elements that carry a net charge, thus creating an electro-osmotic current.

We considered several values of the cylinder diameter, salt concentration, and charge density. The uniform external electric field is kept constant at a value small enough to guarantee that the system is within the linear-response regime.

The Electrokinetic Equations. We utilize the hybrid LB scheme of Capuani et al.[21] to solve the electrokinetic equations on a lattice and with discrete time steps. We refer the reader to ref 21 for further details on this approach.

For the flows that we are considering, the Reynolds numbers are typically very small. Moreover, we can assume that local thermodynamic equilibrium holds, i.e., the microions become thermally equilibrated within the hydrodynamic time scale, $t_{\mathrm{hydr}} \equiv L^2/\nu$, where ν is the kinematic viscosity of the solvent and L is a characteristic length over which the velocity of the solvent varies.

The electrostatic potential is computed by solving the Poisson equation

$$\nabla^2\phi = -4\pi l_{\mathrm{B}}[\sum_{k=\pm} z^k(\rho^k + \rho^{k,\mathrm{W}})], \quad k = +, - \qquad (1)$$

where $\phi \equiv \beta \mathrm{e}\hat{\phi}$ is the electrostatic potential, $\hat{\phi}$, in units of $k_{\mathrm{B}}T/\mathrm{e}$, e is the fundamental charge, $\beta \equiv (k_{\mathrm{B}}T)^{-1}$, $l_{\mathrm{B}} \equiv \mathrm{e}^2\beta/(4\pi\epsilon)$ is the Bjerrum length, and $z^k\rho^k$ and $z^k\rho^{k,\mathrm{W}}$ are the charge densities of the microions (in solution) and of the embedded in solid objects, respectively. z^k is the valence of species k. We solved this equation in real space on the same lattice that was employed to solve the solvent hydrodynamics, using a successive over-relaxation method.[24] This approach allows great flexibility in the choice of the boundary conditions as long as they can be resolved on the lattice.

The time evolution of microion densities are governed by a convection-diffusion equation

$$(\partial_t + \mathbf{u}\cdot\nabla)\rho^k + \nabla\cdot\mathbf{j}^k = 0 \qquad (2)$$

where the ion fluxes (i.e. the number of ions crossing a unit area per unit time) are $\mathbf{j}^k \equiv -D^k\nabla\rho^k + \mu^k\rho^k\mathbf{F}^k$ (D^k and $\mu^k = \beta D^k$ are the relevant diffusion and mobility coefficients, respectively), and **u** is the solvent velocity. The first term corresponds to Fickian diffusion, the second to drift under the influence of a local electric force $\mathbf{F}^k \equiv -(\mathrm{e}z^k)\nabla\hat{\phi}$. In our simulations, we impose strict local mass and charge conservation.[21] The Poisson−Boltzmann approximation prescribes that, in the absence of external forces, the ion densities relax to a canonical thermodynamic equilibrium, $\rho^{k,\mathrm{eq}} = \rho_0 \exp(-z^k\phi)$, where ρ_0 is the salt concentration in the bulk. In fact, in our model, the stationarity implied by the equilibrium distribution is automatically satisfied as we impose that $\mathbf{j}^k$ vanishes for $\rho^k = \rho^{k,\mathrm{eq}}$.

We assume that nonslip boundary condition for the flow field **u** on both the colloidal surfaces and the walls. The assumption of no slip is reasonable as all surfaces involved in our study are, in fact, rough on an atomic scale. As has been shown by Bocquet and Barrat,[32] a very small amount of roughness is enough to cause no-slip behavior on solid surfaces that are wetted by the fluid. For reasons of computational convenience, we choose a kinematic viscosity of $\nu = 1/6$ (in lattice units, l.u.). We choose the solvent density $\rho = 1$. The external (electric) field is chosen to be 10^{-6} (in reduced units). This value is well inside the linear-

response regime. The diffusivity of all microions is set to $D = 0.19$, a value for which spurious diffusion due to lattice advection (see ref 21) is negligible.

III. Tests for Weakly and Highly Charged Rods

Before discussing the transport properties of our model, we briefly describe a few tests that we carried out to verify that our numerical scheme correctly reproduces the equilibrium profile of the electrical double layer in the limit of both a weakly and a highly charged rod of finite length. For the weakly charged case, we can compare the profiles to the analytical solution of the linearized Poisson−Boltzmann equation around an infinite cylinder. For the highly charged case, we verify that our model reproduces Manning condensation.

For an infinite cylinder of radius a and linear charge density ξ, the linearized Poisson−Boltzmann equation $\nabla^2\phi = \kappa^2\phi$ can be solved analytically. Here $\kappa^{-1} \equiv \lambda_D \equiv (8\pi l_B z^2 \rho_0)^{-1/2}$ is the Debye length. In cylindrical coordinates, this equation reduces to $r^{-1}\partial_r(r\partial_r\phi) = \kappa^2\phi$, with the boundary condition $2\pi a\partial_r\phi|_{r=a} = \xi/\epsilon$. Its solution is $\phi(r) = (2\pi\epsilon)^{-1}Cf(r)$, where $C \equiv \xi/\kappa a$ and $f(r) \equiv K_0(\kappa r)/K_1(\kappa a)$, while K_0 and K_1 are the modified Bessel functions. Inserting this solution into the expression for the equilibrium densities $\rho^{\pm,eq}$ and expand to lowest order in $\phi \ll 1$ ("weak charging"), we obtain

$$\rho^{\pm,eq}(r) = \rho_0\left(1 \mp 2\frac{l_B}{e}Cf(r)\right) \tag{3}$$

This symmetric form around $\rho^{\pm,eq}(r) = \rho_0$ is a signature of the Debye−Hückel (linearized Poisson−Boltzmann) regime.

Figure 2 shows the computed density profiles of co- and counterions near a weakly charged cylinder ($\xi l_B/e = 0.07$). As can be seen from the figure, the numerical results are in excellent agreement with the results obtained of the linearized theory (eq 3). Of course, the accuracy of the lattice model improves as the lattice resolution is increased. However, the good match of Figure 2 was obtained with a fairly coarse-grained description (the diameter of the cylinder corresponded to 8 lattice units).

Manning Condensation. For higher line-charge densities (as is the case for DNA with a bare line-charge density of −2e/0.34 nm), the system enters a nonlinear regime where the deviations of ion profiles from their bulk values are no longer antisymmetric under charge reversal. As our simulations solve the nonlinear Poisson−Boltzmann equation, $\nabla^2\phi = 8\pi ez\rho_0\epsilon^{-1}\sinh(z\phi)$, we should expect to reproduce Manning condensation, an intrinsically nonlinear phenomenon that arises for highly charged cylinders in the limit of low salt concentrations, $\lambda_D \gg a$.[25−27]

The Manning parameter is defined as the number of charges in a length l_B on the rod, $q_0 \equiv \xi l_B/e$. There exists a critical value $q_c = 1$ above which the cylinder exerts such strong force on the counterions that these segregate into a condensed-phase layer close to the cylinder, plus a mobile, gaslike phase outside of this layer. The radius of this "Manning cloud" is $R_M = A(a\lambda_D)^{1/2}$, where A depends only weakly on q_0.[28] The effect of the counterions is to renormalize the bare charge of the rod to a universal value e/l_B.

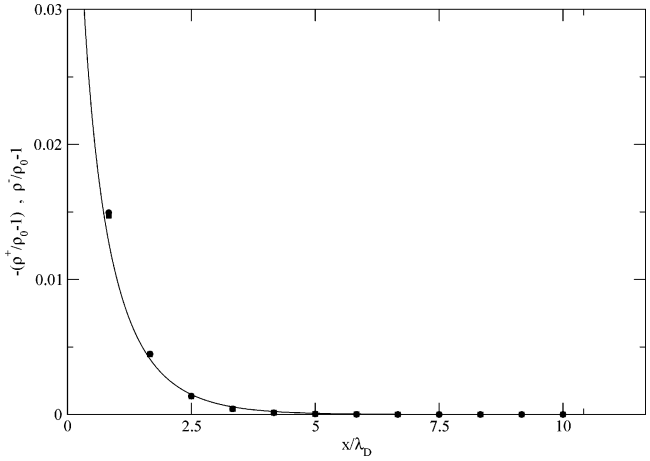

Figure 2. Ion density profiles near a uniformly charged cylinder of finite length, as a function of radial distance to the surface of the cylinder. The reduced charge density per unit length is $\xi l_B/e = 0.07$ (small positive charge density). Both charge density profiles are measured far away from the endpoints of the cylinder, and charge densities are normalized to their value in the bulk (salt concentration). Radial distances are expressed in units of the Debye screening length. The symbols denote simulation results ($\lambda_D/d = 0.15$) for counterions (spheres) and co-ions (squares); solid curves are solutions to the linearized Poisson−Boltzmann equation for an infinite cylinder, see eq 3.

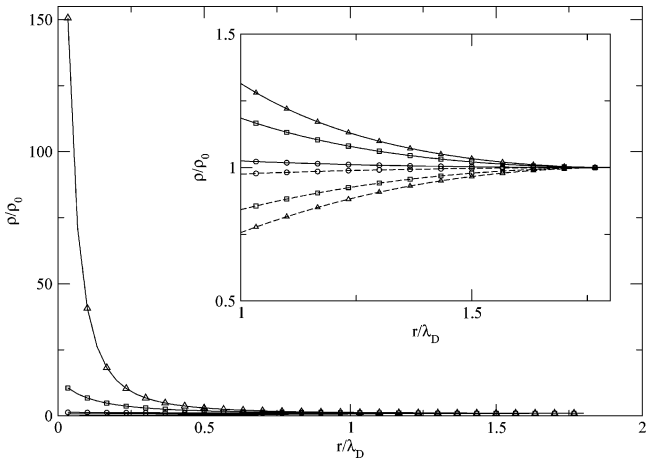

Figure 3. Ionic density profiles near a highly charged cylinder for different values of the Manning parameter q, namely 0.07 (circles), 0.7 (squares), and 2.8 (triangles). Curves are guides to the eye: solid curves represent counterions, dashed curves co-ions. Densities are normalized by their value in the bulk (salt concentration); the distance is normalized by the Debye screening length, $\lambda_D/d = 1.5$. The Manning radius is $R_M/\lambda_D \approx 1$. The inset shows the density profiles for $r > R_M$.

In Figure 3 we show the computed charge density profiles for different line charges: note the symmetry in the profiles for distances above $r/\lambda_D \approx 1$. In Figure 4 we report the values of the counterion concentration, both within and outside the Manning layer $r < R_M$, as a function of q. (Here, q is the Manning parameter resulting from redefining ξ as the linear charge density observed at a distance r from the rod.) Within the Manning layer, the counterion concentration increases roughly quadratically with q, in agreement with analytical

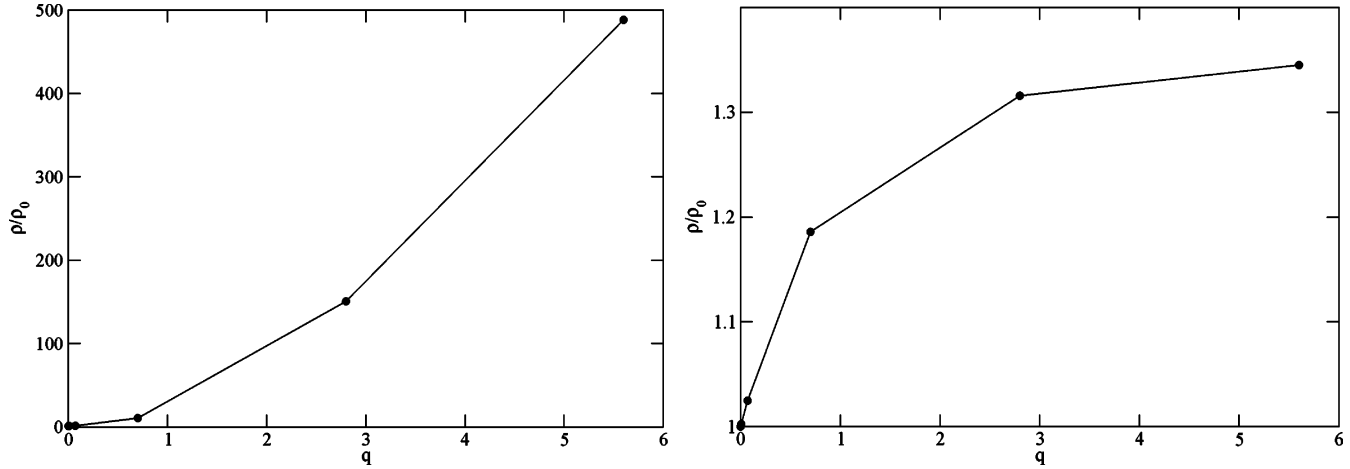

Figure 4. Counterion concentration for different values of the Manning parameter q. Left, within the Manning layer, $r < R_M$; right, outside the Manning layer, $r > R_M$. Symbols are simulation results; curves are guides to the eye. Densities are normalized by the value in the bulk. $\lambda_D/d = 1.5$ and $R_M/\lambda_D \approx 1$.

predictions, whereas outside the Manning layer the counterion concentration is less sentitive to charge increase for $q > 1$. This saturation effect is one of the signatures of Manning condensation. The fact that we do not reach a complete saturation in the counterion concentrations is consistent with the fact that our simulations are performed at small but finite salt concentrations, whereas Manning condensation is a low-salt effect.

IV. Current Modulation during Translocation: Symmetric Pore

Next, we consider the effect of the translocation of a charged rodlike polymer on the ionic currents through the pore. In our simulations, we placed a charged polymer at various positions in or near the translocation pore. We then first equilibrated the charge distributions around the charged polymer. Subsequently, we applied an electric field in a direction parallel to the polymer axis. Immediately after the field is switched on, we observe the onset of electro-osmotic currents. We let the system evolve until these current had reached their steady-state value. We then measure the ionic current, I, as the superposition of conductive plus convective contributions (in the remainder, we assume monovalent ions, $z = 1$, with the same mobility, μ, and we use the elementary charge as our unit of charge: $e = 1$)

$$I \equiv \int\int_{x=\text{const}} \mathrm{dydz}\,[-\mu(\rho^+ - \rho^-)\nabla\phi + (\rho^+ - \rho^-)u_x(y, z)] \tag{4}$$

where μ is the ion mobility and $u_x(y, z)$ is the component of the flow velocity parallel to the symmetry axis. Since mass and charge are conserved to machine precision, and since, in steady state, the total ionic current is a constant along axis Ox, the integral can be taken over any section perpendicular to Ox. To increase precision, we averaged over all planes Oxy. It is worth noting that, for the electric fields used in these simulations, the convective contribution to the current becomes negligible compared to the conductive term.

We measured I for several values of the rod's position, x/l_c, for two values of the screening length, $\lambda_D/d = 1$, 50, and four values of the surface charge densities, $\sigma/(e/d^2) = 0$, 0.1, 0.5, 1. We fixed the rod-to-pore diameter ratio at a value of 1/3. We chose the rodlike polymer to be twice as long as the pore. In Figure 5 we show how the ionic current varies with the position of the translocating polymer. Not surprisingly, we find that if the polymer is uncharged, I invariably decreases as the polymer enters the pore. In other words: the polymer simply blocks part of the current flow. The situation changes when we consider charged polymers. In the high-salt case, $\lambda_D/d = 1$, Figure 5 left, the presence of the polymer in the pore leads to a reduction of the ionic current, but the effect is smaller for highly charged polymers. However, in the low-salt case, $\lambda_D/d = 50$, Figure 5 right, the ionic current I is actually *increased* when a charged polymer is introduced into the pore.

This counterintuitive behavior has recently been observed in experiments[9,29] and large-scale atomistic simulations[10] of DNA 'unsteady' translocation, i.e., electrophoretic translocation of one free DNA oligomer in solution. The advantage of the current approach is that we can separate true steady-state effects from transients that are also present during rapid translocation. In fact, in the atomistic simulations of ref 10 the current enhancement is interpreted as a transient that occurs when DNA leaves the pore: it was attributed to the release of co- and counterions that had accumulated while the DNA was blocking the pore. However, even in ref 10 there is indirect evidence for the effects that we report here, as Figures 4 and 5 in ref 10 also show current enhancement just *before* double-stranded DNA enters the pore.

Figure 6 shows the computed electric current for a neutral polymer with different diameters. The figure shows that the current is proportional to the accessible cross section of the pore. As a consequence, the drop in the current intensity due to the cylinder entering in the pore (defined as the ratio of the currents measured as the cylinder is respectively far from and inside the pore) is proportional to $(d/D)^2$.

This rather trivial effect is nevertheless of practical importance as it is at the basis of experimental techniques

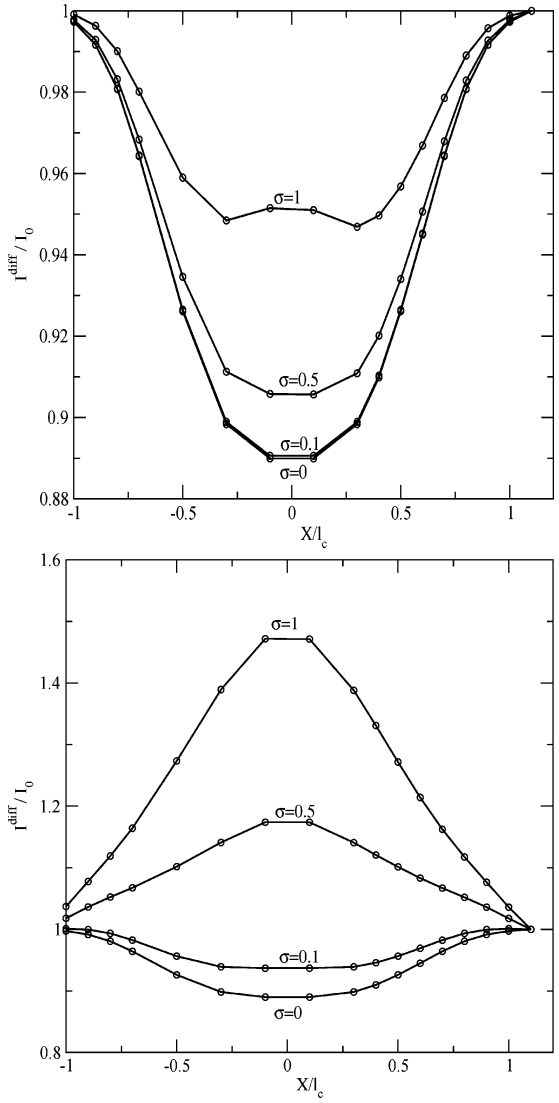

Figure 5. Diffusive ionic current measured at steady state as a function of the cylinder's position X from the pore. Intensities are normalized by the current measured when the cylinder is far from the pore. Results are shown for $\lambda_D/d = 1$ (left) and $\lambda_D/d = 50$ (right) and for different cylinder's surface charge σ. Symbols denote simulation results, while curves are guides to the eye.

to detect the translocation of rodlike macromolecules through a pore. This effect becomes more pronounced as the diameter of the pore becomes comparable to that of the cylinder, which is often the case of in the case of DNA translocation in vivo.

The behavior shown in Figure 5 is due to a competition between these two opposing effects. At low charge, the geometrical effect dominates. But when the cylinder is highly charged and the Debye screening length is large, the electrostatic effect is larger than that due to geometry, and the ionic current is enhanced with respect to the case where the nanopore is empty.

To understand the dependence of the ionic current I on the charge of the translocating polymer, we can use the following rough estimate. We assume that the electric field E and the charge densities ρ^+ and ρ^- are constant inside the pore. If the gap between the cylinder and the pore wall is small, we can approximate this gap by a flat slit. This allows

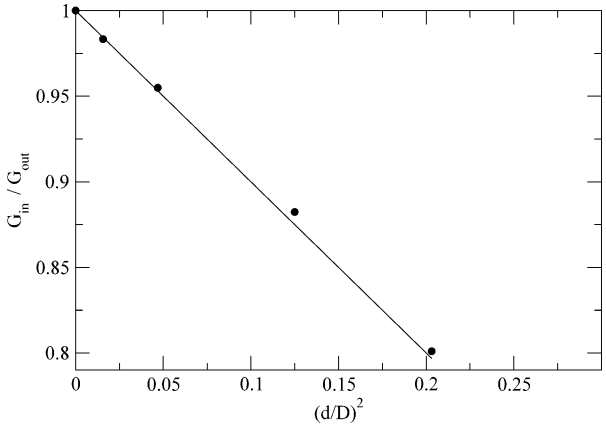

Figure 6. Drop of the conductivity of a nanopore as a function of the cylinder-to-pore cross-section ratio, for an uncharged cylinder. Symbols denote simulation results, and the line is described by the function $1 - (d/D)^2$. The conductivity is proportional to the cross-section of the gap between the pore and the rod.

us to use a simple analytical approximation[30] to estimate the total ionic concentration, $\rho^{+,W} + \rho^{-,W}$, at the pore wall

$$(\rho^{+,W} + \rho^{-,W}) = (\rho_0^+ + \rho_0^-) + \beta\frac{\sigma^2}{2\epsilon} = 2\rho_0\left(1 + \beta\frac{\sigma^2}{4\epsilon\rho_0}\right) \quad (5)$$

Here, $\rho_0^- = \rho_0^+ = \rho_0$ is the concentration of the two species at infinity, and ρ_0 is the salt concentration in the solution bulk.

Using this approximation, we can estimate the relative variation of the current intensity due to the surface charges, by using eq 5, and obtain

$$\frac{I(\sigma, \rho_0)}{I(\sigma = 0, \rho_0)} = 1 + \beta\frac{\sigma^2}{4\epsilon\rho_0}$$

Hence, recalling that $\lambda_D \equiv (8\pi l_B \rho_0)^{-1/2}$ and $l_B \equiv e^2\beta/(4\pi\epsilon)$, we obtain

$$\frac{\Delta I}{I_0} \equiv \frac{I(\sigma, \rho_0) - I(0, \rho_0)}{I(0, \rho_0)} = 8\pi^2\left(\frac{\sigma\lambda_D l_B}{e}\right)^2 \quad (6)$$

We can combine the effects of geometry and surface charge in one single (approximate) expression

$$\frac{\Delta I}{I_0} = \frac{I(\sigma, \rho_0) - I_0(0, \rho_0)}{I_0(0, \rho_0)} = \left(\frac{D-d}{D}\right)^2\left(1 + 8\pi^2\left(\frac{\sigma\lambda_D l_B}{e}\right)^2\right) - 1 \quad (7)$$

where I_0 denotes the current through the unobstructed pore. Note that sign of ΔI can be either positive or negative, depending on whether translocation enhances or decreases the current through the pore. Equation 7 shows that the ionic current increases with increasing Debye screening length. On the other hand, the partial blocking of the nanopore by the translocating polymer tends to decrease the electric current.

Figure 7 shows the relative variation of the current $\Delta I/I_0$ as a function of the dimensionless parameter $\sigma\lambda_D l_B/e$. As can

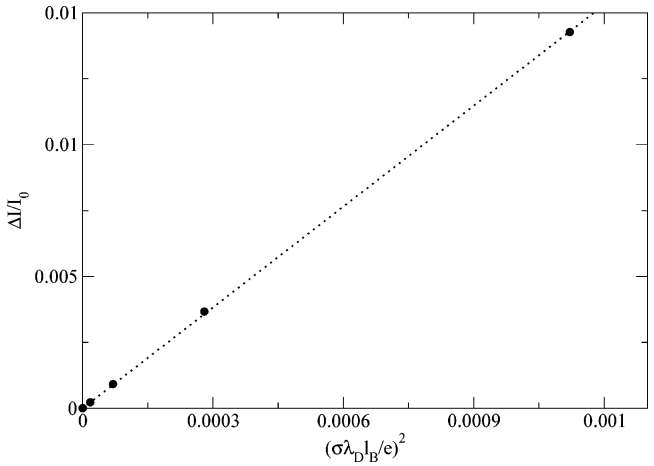

Figure 7. Relative variation of the ionic current, with respect to the ionic current measured for $\sigma = 0$, as a function of the surface charge squared on the cylinder. The surface charge σ is normalized by the length scales λ_D and l_B and the elementary charge e, resulting in a Manning parameter (see text). Symbols denote simulation results for $\lambda_D = 1.5$ and $D - d = 2$ (l.u). The dotted curve shows a quadratic fit to the numerical data, in good agreement with our analytic approximation (see text).

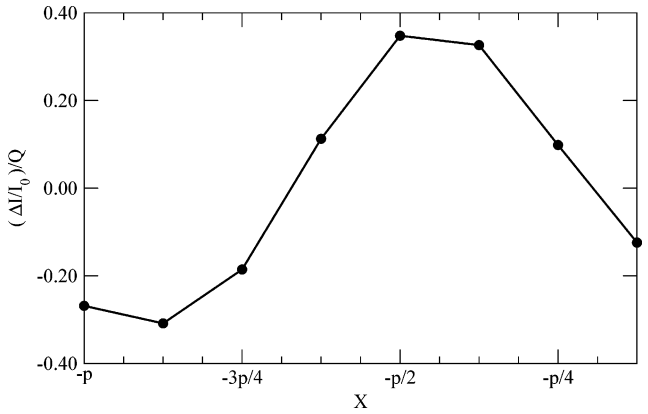

Figure 8. Modulation in the ionic current as ssDNA of radius 5 (l.u.) translocates through a pore of radius 10 (l.u.) at position X, shown as the relative variation $\Delta I/I_0$ of the ionic current with respect to the ionic current I_0, measured for $\sigma = 0$. We normalized this variation to the dimensionless parameter $Q \equiv (\sigma\lambda_D l_B/e)^2$ — this should correct for the explicit dependence of the current on the average charge density of the cylinder (eq 6). The diameters of the ssDNA and the pore are 10 and 20 l.u., respectively, and $p = 8$ l.u. is the helical pitch. Symbols denote simulation results, and the curves are guides to the eye.

be seen from the figure, the numerical data reproduce the quadratic dependence predicted by eq 6.

Of course, in experiments on polyelectrolyte translocation, the (bare) surface charge σ of the polyelectrolyte is dictated by its chemical composition and will usually not be varied. However, it is possible to vary the geometry of the nanopore and, more easily, the concentration of added salt. If we consider typical salt concentrations in the range from 10 mM to 1 M, then our simulations apply to nanopores with typical widths in the range $5 < D < 20$ nm and heights between $10 < h < 40$ nm.

V. Current Modulation during Translocation Past a Charged Probe

The holy grail of experiments on DNA translocation is to extract sequence information from the modulation of the ionic current. Although progress in this direction is certainly being made (see, e.g. ref 31), the generation and interpretation of a DNA translocation "signals" is not straightforward. To study current modulation during DNA translocation, we considered a model polyelectrolyte with constant thickness but a helical (rather than uniform) charge distribution. Translocation of such a helical polyelectrolyte through a symmetric nanopore does not give rise to any current modulation. The reason is that shifting the cylinder by an arbitrary distance h along its axis is equivalent to a rotation of angle $\theta = 2\pi h/p$, where p is the pitch of the helix—and simple rotations of a charged helix in a cylindrically symmetric pore do not change the total current. We therefore considered the interesting case of nanopore with a charged patch that acts as a probe, embedded in the tube wall.

Current nanofabrication techniques allow the production of synthetic pores of the diameter comparable to the thickness of the DNA oligomer (2 nm). Biological pores such as α-hemolysin have similar internal diameters. The design of a nanopore with a charged probe in the wall of the channel is therefore not beyond what is currently feasible. A charged patch acts as a probe because the overlap of the electrical double layers around the patch and the DNA affects the ionic current.

To obtain an estimate of the possible magnitude of such current modulations, we considered single- and double-helix charge distributions on the rod as models for ss- and dsDNA, respectively. As for ssDNA, we placed an infinite cylinder with a single helix charge distribution in the pore and measured the steady-state ionic current in response to a constant voltage for different displacements of the cylinder along its longitudinal axis. The surface charge of the patch was chosen to have the same sign and magnitude as that of the charges on the cylinder, but this assumption is not essential.

Figure 8 shows that, with such an asymmetrically placed probe, the total electric current is indeed modulated upon translocation (or, equivalently, rotation) of the ssDNA rod. In our (discretized) model, the helix pitch was equal to 8 lattice units (l.u.), and hence eight values for the current are reported in Figure 8.

In the case of ssDNA, one might argue that the fact that such molecules have a rather short persistence length (1.5−3 nm) would render the rigid rod model inadequate. However, flexibility would not affect the order of magnitude of the predicted modulations. Moreover, one might envisage situations where the ssDNA is prestretched by linking it to optically trapped colloidal beads on both sides of the pore.

This problem does not occur with the much more rigid double-stranded DNA. We model dsDNA as a cylinder of constant thickness covered by a double helical charge distribution (see Figure 9). We computed similar setups to those for the ssDNA, using the same charge patch inside the pore. To compare the effect of changing configuration

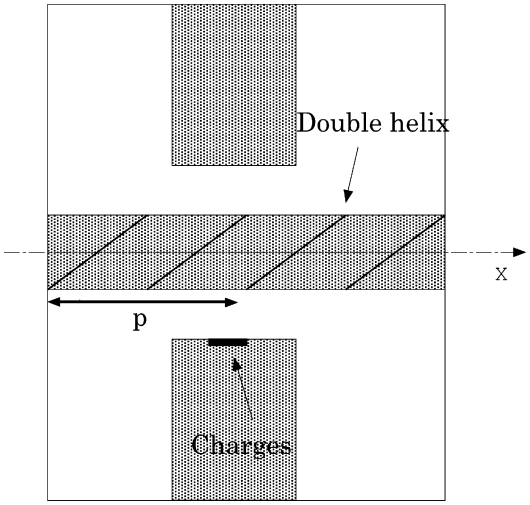

Figure 9. Schematic drawing of the translocation of dsDNA past a charged probe. On the dsDNA, two helical line charges form a double helix. The black area in the pore denotes the charged "probe". X denotes the position of the cylinder and *p* is the pitch of the helix. The ionic current is measured at steady state with a constant voltage bias. The overlap of the electrical double layer around the patch with that around the double helix locally increases the charge density, thus increasing the ionic current with periodicity *p*/2 as the cylinder translocates. A second patch on the opposite side of the pore would enhance the modulations in the current; however, this is only true for radially symmetric charge distributions, such as that of dsDNA.

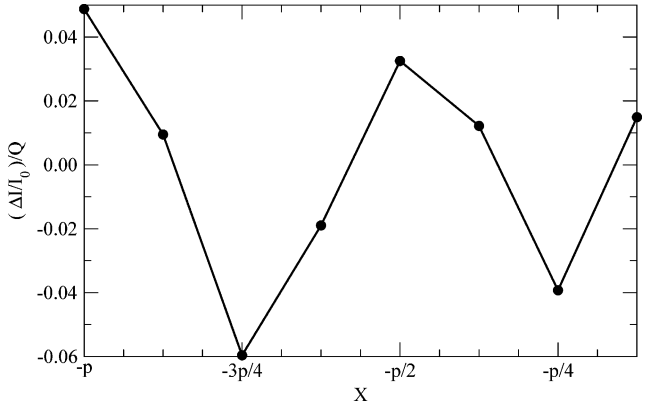

Figure 10. Modulation in the ionic current as dsDNA translocates through a pore at position X, shown as the relative variation of the ionic current with respect to the ionic current I_0, measured for $\sigma = 0$. We normalized this variation to the dimensionless parameter $Q \equiv (\sigma\lambda_D l_B/e)^2$ — this should correct for the explicit dependence of the current on the average charge density of the cylinder (eq 6). The diameters of the dsDNA and the pore are 10 and 20 l.u., respectively, while $p = 8$ l.u. is the helix pitch. The period of the modulations is half of that for ssDNA. Symbols denote the simulation results, and curves are guides to the eye. The actual modulation is much smaller (10^{-4}) than the average current. Hence, small discretization errors show up clearly in this figure: in the absence of such errors the modulation would be perfectly periodic with a period *p*/2.

(from single to double helix), we divide the current modulation by $Q \equiv (\sigma\lambda_D l_B/e)^2$, which should describe the effect of a smeared out charge density σ on the ionic current (eq 6). Our simulations again indicate that the ionic current is modulated upon translocation of the dsDNA (see Figure 10). The period of the modulations is now half the pitch of one helix. The screening length was chosen to be smaller than the pitch and comparable to the size of the charged patch. This choice maximizes the inhomogeneity of the electric potential. For dsDNA, these conditions can be achieved with a 1 M monovalent salt in water at room temperature, which is in the range of experimental parameters. This yields a screening-length of 0.3 nm for a pitch of 3 nm.

The amplitude of the scaled current modulation during translocation is larger (approximately seven times) for the single helix than the double helix. The value of this ratio suggests that the scaled current modulation is not simply proportional to the variance in the surface charge density. We have not attempted to quantify this dependence. Both for ssDNA and dsDNA, the unscaled current modulation is small (typically, between $1{:}10^2$ and $1{:}10^4$). In experiment, such a signal might still be detectable if the position of the DNA is modulated periodically.

We have not attempted to optimize the conditions for maximal modulation of the translocation current. Within the current model, there is certainly room for improvement. For instance, $\Delta I/I_0$ increases with increasing ratio of the diameter *d* of the DNA to the diameter *D* of the pore. In our simulations, the maximum value of *d*/*D* was determined by the lattice resolution. By increasing this resolution, larger *d*/*D* ratios can be studied. However, for DNA fitting snugly in the pore, it would not be justified to ignore the corrugation (grooves) of the DNA surface. Hence, we have not attempted to study this limit.

Conclusions

In summary, we have presented Lattice-Boltzmann simulations of the modulation in ionic current associated with the translocation of charged oligomers through nanopores under an applied electric field. Our first observation is that, depending on the conditions (charge of the polyelectrolyte, ionic strength of the solution), translocation may either decrease or, more surprisingly, increase the ionic current.

In addition, we have presented simulations that indicate that the modulation of the ionic current during translocation can be made sensitive to the microscopic charge distribution of the DNA by placing a localized charged "probe" on the wall of the nanopore. We argue that this effect should be experimentally observable, even though the predicted current modulations are small. Of course, thermal ("Nyquist") noise in the electrical current may partially obscure such measurements. However, unlike the thermal noise, the translocation-induced current modulation increases with increasing current. Moreover, if the DNA is connected to a colloidal bead that is moved periodically, then the signal-to-noise problem can be reduced by employing phase-sensitive detection.

Acknowledgment. The work of the FOM Institute is part of the research program of FOM and is made possible by financial support from The Netherlands Organization for Scientific Research (NWO).

Note Added after ASAP Publication. This article was released ASAP on March 22, 2006, with the incorrect Received Date. The correct version was posted on April 17, 2006.

References

(1) *Electrostatic effects in Soft Matter and Biophysics*; Holm, C., Kèkicheff, P., Podgornik, R., Eds.; NATO Sci. Series, Kluwer Academic Publisher: Dordrecht, 2001.

(2) Gelbart, W. M.; Bruinsma, R. F.; Pincus, P. A. DNA-inspired electrostatics. *Phys. Today* **2000**, *53*, 38−44.

(3) Probstein, R. F. *Physicochemical Hydrodynamics*; Butterworth: Boston, MA, 1989.

(4) Stroock, A. D.; Dertinger, S. K. W.; Ajdari, A.; Mezic, I.; Stone, H. A.; Whitesides, G. M. Chaotic mixer for microchannels. *Science* **2002**, *295*, 647−651.

(5) Kasianowicz, J. J.; Brandin, E.; Branton, D.; Deamer, D. W. *Proc. Natl. Acad. Sci. U.S.A.* **1996**, *93*, 13770−13773.

(6) Li, J.; Stein, D.; McMullan, C.; Branton, D.; Aziz, M. J.; Golovchenko, J. A. Ion-beam sculpting at nanometre length scales. *Nature* **2001**, *412*, 166−169.

(7) JLi, J. L.; Gershow, M.; Stein, D.; Brandin, E.; Golovchenko, J. A. *Nat. Mater.* **2003**, *2*, 611−615.

(8) Storm, A. J.; Chen, J. H.; Zandbergen, H. W.; Dekker, C. Translocation of double-strand DNA through a silicon oxide nanopore. *Phys. Rev. E* **2005**, *71*, 051903.

(9) Chang, H.; Kosari, F.; Andreadakis, G.; Alam, M. A.; Vasmatzis, G.; Bashir, R. DNA-mediated fluctuations in ionic current through silicon oxide nanopore channels. *Nano Lett.* **2004**, *4*, 1551−1556.

(10) Aksimentiev, A.; Heng, J. B.; Timp, G.; Schulten, K. Microscopic kinetics of DNA translocation through synthetic nanopores. *Biophys. J.* **2004**, *87*, 2086−2097.

(11) Heng, J. B.; Ho, C.; Kim, T.; Timp, R.; Aksimentiev, A.; Grinkova, Y. V.; Sligar, S.; Schulten, K.; Timp, G. Sizing DNA using a nanometer-diameter pore. *Biophys. J.* **2004**, *87*, 2905−2911.

(12) Aksimentiev, A.; Schulten, K. Imaging alpha-hemolysin with molecular dynamics: Ionic conductance, osmotic permeability, and the electrostatic potential map. *Biophys. J.* **2005**, *88*, 3745−3761.

(13) Hoogerbrugge, P. J.; Koelman, J. M. V. A. Simulating Microscopic Hydrodynamic Phenomena with Dissipative Particle Dynamics. *Europhys. Lett.* **1992**, *19*, 155−160.

(14) Groot, R. D.; Warren, P. B. Dissipative particle dynamics: Bridging the gap between atomistic and mesoscopic simulation. *J. Chem. Phys.* **1997**, *107*, 4423−4435.

(15) Groot, R. D. Electrostatic interactions in dissipative particle dynamics-simulation of polyelectrolytes and anionic surfactants. *J. Chem. Phys.* **2003**, *118*, 11265−11277.

(16) Malevanets, A.; Kapral, R. Mesoscopic model for solvent dynamics. *J. Chem. Phys.* **1999**, *110*, 8605−8613.

(17) Ihle, T.; Kroll, D. M. Stochastic rotation dynamics: A Galilean-invariant mesoscopic model for fluid flow. *Phys. Rev. E* **2001**, *63*, 020201.

(18) Succi, S. *The Lattice Boltzmann Equation for Fluid Dynamics and Beyond*; University Press: Oxford, 2001.

(19) Ladd, A. J. C. Numerical Simulations of Particulate Suspensions via a Discretized Boltzmann-Equation. 1. Theoretical Foundation. *J. Fluid Mech.* **1994**, *271*, 285−309.

(20) Gonzalez-Segredo, N.; Nekovee, M.; Coveney, P. V. Three-dimensional lattice-Boltzmann simulations of critical spinodal decomposition in binary immiscible fluids. *Phys. Rev. E* **2003**, *67*, 046304.

(21) Capuani, F.; Pagonabarraga, I.; Frenkel, D. Discrete solution of the electrokinetic equations. *J. Chem. Phys.* **2004**, *121*, 973−986.

(22) Thompson, A. P. Nonequilibrium molecular dynamics simulation of electro-osmotic flow in a charged nanopore. *J. Chem. Phys.* **2003**, *119*, 7503−7511.

(23) Alder, B. J.; Wainwright, T. E. Decay of the Velocity Autocorrelation Function. *Phys. Rev. A* **1970**, *1*, 18−21.

(24) Press, W. H.; Teukolski, S. A.; Vetterling, W. T. *Numerical Recipes*; Cambridge University Press: Cambridge, 1996.

(25) Oosawa, F. Interaction between parallel rodlike macroions. *Biopolymers* **1968**, *6*, 1633−1647.

(26) Manning, G. S. Limiting Laws and Counterion Condensation in Polyelectrolyte Solutions I. Colligative Properties. *J. Chem. Phys.* **1969**, *51*, 924−933.

(27) Manning, G. S.; Ray, J. Counterion condensation revisited. *J. Biomol. Struct. Dyn.* **1998**, *16*, 461−476.

(28) O'Shaughnessy, B.; Yang, Q. Manning-Oosawa counterion condensation. *Phys. Rev. Lett.* **2005**, *94*, 048302.

(29) Smeets, R.; Keyser, U.; Krapf, D.; Wu, M. Y.; Dekker, N.; Dekker, C. *Preprint*, 2005.

(30) Israelachvili, J. N. *Intermolecular and Surface Forces;* Academic Press: New York, 1991.

(31) Vercoutere, W. A.; Winters-Hilt, S.; DeGuzman, V. S.; Deamer, D.; Ridino, S. E.; Rodgers, J. T.; Olsen, H. E.; Marziali, A.; Akeson, M. Discrimination among individual Watson−Crick base pairs at the termini of single DNA hairpin molecules. *Nucleic Acids Res.* **2003**, *31*, 1311−1318.

(32) Bocquet, L.; Barrat, J. L. *Phys. Rev. Lett.* **1993**, *70*, 2726.

(33) Butler, J. C.; Angelini, T.; Tang, J. X.; Wong, G. C. L. *Phys. Rev. Lett.* **2003**, *91*, 028301.

(34) Bostrom, M.; Williams, D. R. M.; Ninham, B. W. *J. Phys. Chem. B* **2002**, *106*, 7908.

CT050340G